PAK3 mutations responsible for severe intellectual disability and callosal agenesis inhibit cell migration

Kévin Duarte, Solveig Heide, Sandrine Poea-Guyon, Veronique Rousseau, Christel Depienne, Agnès Rastetter, Caroline Nava, Tania Attié-Bitach, Ferechté Razavi, Jelena Martinovic, et al.

Neurobiology of Disease 136 (2020) 104709

Contents lists available at ScienceDirect

Neurobiology of Disease

journal homepage: www.elsevier.com/locate/ynbdi

PAK3 mutations responsible for severe intellectual disability and callosal agenesis inhibit cell migration

Kévin Duarte[a], Solveig Heide[b,1], Sandrine Poëa-Guyon[a,1], Véronique Rousseau[a], Christel Depienne[b,c], Agnès Rastetter[b], Caroline Nava[b], Tania Attié-Bitach[d], Ferechté Razavi[d], Jelena Martinovic[e], Marie Laure Moutard[f], Jacqueline Cherfils[g], Cyril Mignot[b], Delphine Héron[b,**], Jean-Vianney Barnier[a,*]

[a] Department of Cognition and Behavior, Paris-Saclay Institute of Neuroscience (Neuro-PSI CNRS, UMR 9197), Paris-Sud and Paris-Saclay Universities, Orsay, France
[b] Department of genetics, Reference Center for Intellectual Disabilities of Rare Causes, APHP, GH Pitié Salpêtrière, Paris, France
[c] Institute of Human Genetics, University Hospital Essen, University of Duisburg-Essen, Essen, Germany
[d] Unité d'Embryofoetopathologie, Service of Histology-Embryology-Cytogenetics, APHP Necker Enfants Malades & Imagine Institute, Inserm U1163, Paris, France
[e] Unité de foetopathologie, APHP Antoine Béclère, Paris, France
[f] Department of Pediatrics Neurology, Reference Center for Intellectual Disabilities of Rare Causes APHP, Armand-Trousseau Hospital, Paris, France
[g] Laboratoire de Biologie et Pharmacologie Appliquée, CNRS and Ecole normale supérieure Paris-Saclay, Cachan, France

ARTICLE INFO

Keywords:
Corpus callosum agenesis (CCA)
Cell adhesion
Cell migration
Cell spreading
Intellectual disability
Kinase
Neurodevelopmental disorder
PAK3
αPIX/ARHGEF6

ABSTRACT

Corpus callosum agenesis (CCA) is a brain malformation associated with a wide clinical spectrum including intellectual disability (ID) and an etiopathological complexity. We identified a novel missense G424R mutation in the X-linked p21-activated kinase 3 (*PAK3)* gene in a boy presenting with severe ID, microcephaly and CCA and his fetal sibling with CCA and severe hydrocephaly. PAK3 kinase is known to control synaptic plasticity and dendritic spine dynamics but its implication is less characterized in brain ontogenesis. In order to identify developmental functions of *PAK3* impacted by mutations responsible for CCA, we compared the biochemical and biological effects of three *PAK3* mutations localized in the catalytic domain. These mutations include two "severe" G424R and K389N variants (responsible for severe ID and CCA) and the "mild" A365E variant (responsible for nonsyndromic mild ID). Whereas they suppressed kinase activity, only the two severe variants displayed normal protein stability. Furthermore, they increased interactions between PAK3 and the guanine exchange factor αPIX/ARHGEF6, disturbed adhesion point dynamics and cell spreading, and severely impacted cell migration. Our findings highlight new molecular defects associated with mutations responsible for severe clinical phenotypes with developmental brain defects.

1. Introduction

The corpus callosum is the main myelinated fiber tract in the human brain commissures between homotopic and heterotopic regions of the cerebral hemispheres. Its development begins early during brain ontogenesis, from the 13th to 20th weeks after conception (Edwards et al., 2014). Corpus callosum agenesis (CCA) is among the most common brain morphological anomalies affecting about one out of 4000 newborns and its prevalence reaches 2–3% of individuals with intellectual disability (ID) (Grogono, 1968; Schaefer and Bodensteiner, 1992; Wang et al., 2004). CCA is extremely heterogeneous both clinically and etiologically. Genetic causes are usually identified in 30–45% of CCA,

* Correspondence to: J.-V. Barnier, Department of Cognition and Behavior, Paris-Saclay Institute of Neuroscience (Neuro-PSI CNRS, UMR 9197), Paris-Sud and Paris-Saclay Universities, 91400 Orsay, France.
** Correspondence to: D. Héron, Department of Genetics, Reference Center for Intellectual Disabilities of Rare Causes, APHP, GH Pitié Salpêtrière, 75013 Paris, France.
E-mail addresses: Kevin.duarte@u-psud.fr (K. Duarte), Solveig.heide@aphp.fr (S. Heide), Sandrine.guyon@u-psud.fr (S. Poëa-Guyon), Veronique.rousseau@u-psud.fr (V. Rousseau), Christel.depienne@uni-due.de (C. Depienne), Agnes.rastetter@icm-institue.org (A. Rastetter), Caroline.nava@aphp.fr (C. Nava), Tania.attie@inserm.fr (T. Attié-Bitach), Marielaure.moutard@trs.aphp.fr (M.L. Moutard), Jacqueline.cherfils@ens-cachan.fr (J. Cherfils), Cyril.mignot@aphp.fr (C. Mignot), Delphine.heron@aphp.fr (D. Héron), jean-vianney.barnier@u-psud.fr (J.-V. Barnier).
[1] Solveig Heide and Sandrine Poëa-Guyon contributed equally to this study.

https://doi.org/10.1016/j.nbd.2019.104709
Received 9 May 2019; Received in revised form 13 November 2019; Accepted 8 December 2019
Available online 14 December 2019

including chromosomal rearrangements (10–20%) and Mendelian conditions (30%) (Edwards et al., 2014; Palmer and Mowat, 2014). Several chromosomal alterations and > 300 different causative genes have been reported to date (Edwards et al., 2014; Heide et al., 2017). However, in a relatively large proportion of cases, the genetic defect remains unidentified. We report here a new likely causative mutation p.Gly424Arg (G424R) in the X-linked p21-activated kinase *PAK3* gene in a patient with CCA and severe ID, and in his sibling fetus with hydrocephaly and CCA.

More than ten *PAK3* mutations have been reported to date in mild to severe ID with or without brain anomalies such as microcephaly, macrocephaly, and callosal agenesis (Allen et al., 1998; Bienvenu et al., 2000; Cartwright et al., 2017; Gedeon et al., 2003; Hertecant et al., 2017; Horvath et al., 2018; Magini et al., 2014; McMichael et al., 2015; Muthusamy et al., 2017; Peippo et al., 2007; Rejeb et al., 2008). PAK3 belongs to the family of the p21-activated kinases which are downstream effectors of the RAC and CDC42 GTPases and control cytoskeleton dynamics, cell movement and migration, as well as cell proliferation (Bokoch, 2003). Even if PAK3 is already known as a key regulator of synaptic plasticity and dendritic spine dynamics, its precise role in neurodevelopmental processes remains elusive (Kreis and Barnier, 2009).

PAK3 is a multi-functional protein whose functions depend on its kinase activity and on its different substrates. It also possesses scaffolding functions with partners involved in signalling pathways (Kreis and Barnier, 2009). Several biochemical defects related to pathogenic variants have been characterized including alteration of its kinase activity, protein stability, GTPase binding, dimer formation, and MAPK activation (Combeau et al., 2012; Kreis et al., 2007; Magini et al., 2014; Thévenot et al., 2011). In order to elucidate the genotype-phenotype relationship of affected patients, and more precisely to decipher the molecular bases of *PAK3*-mediated CCA, we performed a comparative analysis at the structural, biochemical and cellular levels between two mutation types: i) two missense mutations, K389N and the new G424R mutation, both responsible for severe ID and brain anomalies including microcephaly and CCA and ii) another missense mutation, A365E, responsible for nonsyndromic mild ID (Gedeon et al., 2003; Magini et al., 2014). These three mutations are located in the C-terminal lobe of the kinase domain but outside the catalytic site. We analysed their phylogenic conservation, impact on protein structure and their consequences on catalytic functions. In this study, we also demonstrate that although these three mutations totally suppress PAK3 catalytic activity, only the two mutations causing severe ID and CCA maintain a wild-type (WT)-like protein stability, increase αPIX/ARHGEF6 binding, impair adhesion point dynamics, and inhibit cell migration.

Our results therefore suggest a new molecular defect associated with PAK3 mutations leading to severe ID and CCA that may be partly responsible for cell migration defects and brain morphological abnormalities.

2. Materials and methods

2.1. Editorial policies and ethical considerations

Written informed consent was obtained for all participants of this family. The research was approved by the local ethics committee.

2.2. Genomic analysis

DNA of the patient isolated from blood sample was sequenced in trio with healthy parents. The Roche/Nimblegen v3 exome, 64 Mb kit was used for library preparation with 12 samples multiplexing, according to manufacturer's protocol. This library was then sequenced on a NextSeq 500 (Illumina) with a 2x150bp high output flowcell. The bioinformatic analyses were conducted by Polyweb using BWA 0.7.12, picard-tools-1.121, GenomeAnalysisTK-2014.3- 17-g0583013, SNPEff-4.2. The identified *PAK3* variant was then confirmed by Sanger sequencing in the proband, the sibling fetus and their mother. We performed familial segregation by Sanger sequencing in a healthy maternal uncle. Probes are available upon request.

2.3. In silico analysis

In silico prediction analyses were assessed by using SIFT/Provean, Polyphen-2, and mutation taster (Adzhubei et al., 2013; Kumar et al., 2009; Schwarz et al., 2014). NM_001128166 transcript sequence from NCBI and ENSP00000361077 protein sequence from Ensembl version 93 were used for this study (Zerbino et al., 2018). Common variants of this mutation were investigated by analyzing 1000 Genome Project, gnomAD (genome aggregation database), and Database of Single Nucleotide Polymorphism (dbSNP) databases (1000 Genomes Project Consortium et al., 2012; Sherry et al., 2001). Analysis of Φ and ψ angles was done using RAMPAGE server (Lovell et al., 2003). The PAK3 3D structure referred as PDB entry 6FD3 and the unphosphorylated activation loop taken from the structure of unphosphorylated PAK1 (PDB entry 3Q4Z) were extracted from Protein Data Bank and modeled with PyMOL (Sorrell et al., 2019; Wang et al., 2011).

2.4. Mutagenesis and plasmids

The following plasmids were previously described: pcDNA3-HA-PAK3-WT encodes the HA-tagged wild type PAK3 protein, the pcDNA3-HA-PAK3-K297L encodes K297L kinase dead mutant and pcDNA3-HA-PAK3-A365E encodes a ID-mutated PAK3 variant (Kreis et al., 2007; Rousseau et al., 2003). The two mutants PAK3-K389N and PAK3-G424R were generated from pcDNA3-HA-PAK3-WT plasmid with Q5 high-fidelity DNA polymerase (NEB, #M0491S) by PCR and the primers set (5'-CCAAGTGATCCACAGAGACATAAATAGCGACAACATTCTCC TCG-3′ and 5'-CGAGGAGAATGTTGTCGCTATTTATGTCTCTGTGGATC ACTTGG-3′) and the primer set (5'-GTAAACGAAGCACTATGGTGAGA ACTCCCTATTGGATGGCAC-3′ and 5'-GTGCCATCCAATAGGGAGTTCT CACCATAGTGCTTCGTTTAC-3′), respectively using Quick change mutagenesis protocols. Mutated *PAK3* gene sequences were verified by sequencing (Eurofins-GATC Company). The PIX interaction mutant (PIM) pcDNA3-HA-PAK3-P194G-R195A was generated from pcDNA3-HA-PAK3-WT using a Phusion site-directed mutagenesis kit (Thermofischer #F541) with the oligonucleotide set (5'-GGAGCTCCAGAGCAT ACAAAATCAATCTATACTCGC-3′ and 5'-TGCAATGACAGGCGGGGG TTC-3′). Lentiviral vectors (pHAGE-HA-PAK3) used for COS7 cells infection were derived from pHAGE backbone using a "Gateway"® cloning protocol (Invitrogen) by introducing specific AttB sequences using the pcDNA3-HA-PAK3 plasmids as templates (WT, K297L, A365E, K389N and G424R) and the oligonucleotide set (5'-GGGGACAAGTTT GTACAAAAAAGCAGGCTTCACCATGGCTAGCTATCC-3′ and 5'-GGGGA CCACTTTGTACAAGAAAGCTGGGTGTCTAGACTAACGGCTACTG TTC-3′) (Murphy et al., 2006). Then a specific recombination (BP cloning step) between AttB-PCR products and the pDONR221 plasmid was performed using the BP clonase enzyme (Invitrogen, #12–535-029). The resulting pENTR-HA-PAK3 plasmids were used with LR clonase enzyme (Invitrogen, #11791-020) in addition to the pHAGE backbone (LR cloning step) to generate the lentiviral vectors (pHAGE-HA-PAK3). The *PAK3* coding sequences cloned in these pHAGE-HA-PAK3 were finally verified by sequencing.

2.5. Cell culture, transfection, virus production and infection

COS7 cells and HEK 293T cells were cultured in Dulbecco's modified Eagle's medium (Gibco, #31966-020) supplemented with 10% fetal bovine serum (FBS), 100 U/mL penicillin and 100 µg/mL streptomycin. HEK cells (used for kinase assay and protein interaction assay) were plated at 8.10^6 cells/100 mm dish and transfected with 30 µg of plasmid DNA (10 µg of pcDNA3-HA-PAK3 + 10 µg of carrier, in

combination with 10 μg of either pGFP-CDC42-V12, pGFP-CDC42-N17, pFLAG-*α*PIX, or pFLAG-*β*PIX) using a calcium-phosphate protocol. After 12 h of transfection, medium was changed with a fresh one and cells were then starved during 24 h with 0.5% FBS. Cell lines for each variant were established as follow: the different virus supernatants were produced in HEK cells by transfection of the pHAGE-HA-PAK3 variant plasmids, with the PAX2 gag-pol and the VSVg envelop pMD2 plasmids using lipofectamine-2000 (Invitrogen, #11668030). After 2 days, the viral suspension was filtered with a 0.45 μm filter and was then added on COS7 cells. Seventy-two hour after infection, transduced cells were selected by addition of 0.5 mg/mL of Geneticin (Sigma, #G8168) for 8 days. In these established COS7-Lv-PAK3 cell lines, expression of PAK3 variants was induced by doxycycline treatment (2 μg/mL, Sigma). PAK3 expression reaches maximal value as soon as 24 h of doxycycline treatment (data not shown).

2.6. Biochemical assays

For kinase assay, HA-PAK3 mutant proteins were coexpressed in HEK cells either with a constitutively active GTP-loaded form of the CDC42 (CDC42-V12) or with a dominant-negative GDP-loaded mutant (CDC42-N17). Thirty-six hours later, cells were washed twice with ice-cold phosphate buffered saline (PBS) supplemented with 0.1 mM orthovanadate and lysed in cold lysis buffer containing 50 mM Tris-HCl pH 7.5, 1% Triton X-100, 100 mM NaCl, 50 mM NaF, 10 mM $Na_4P_2O_7$, 5 mM EDTA, 1% aprotinin supplemented with protease and phosphatase inhibitors mixture. PAK3 proteins were HA-affinity purified, washed as previously described and washed one more time with kinase buffer (25 mM HEPES pH 7.4, 25 mM $MgCl_2$ and 25 mM *β*-glycerophosphate). Immunoprecipitates were incubated in kinase buffer containing 40 μM ATP and 5 μCi of [γ-^{32}P] ATP for 20 min at 30 °C in presence of 3 μg of myelin basic protein (MBP) as a substrate. Samples were then boiled in SDS-Laemmli buffer to stop the reaction and the products were resolved by 12% SDS-PAGE. Gels were dried and exposed to autoradiography. Immunoblot analysis were performed using anti-GFP (Millipore, #MAB3580), anti-*β*PAK (N-19, Santa Cruz, #SC-1871), anti-HA (Cell Signaling Technology, #2367). Membranes were then incubated using anti-mouse (Biorad, #172-1011), anti-goat (Pierce, PA1-86326) and/or anti-rabbit (Biorad, #75011) peroxidase-linked secondary antibodies. Membranes were then revealed with Luminata Crescendo (Millipore).

To assess the protein stability, *PAK3* expression was induced by doxycycline in COS7-Lv-PAK3 cells during 48 h. PAK3 protein synthesis was stopped by doxycycline withdrawal, cells were lysed at the indicated time and decrease of PAK3 protein level was monitored by western blot on 10 μg of Total cell lysates (TCL) proteins as described above, using anti-HA antibodies and with anti-α-tubulin (Sigma, T6199) western blot as loading control. For MAP Kinase activation, *PAK3* expression in Lv-transduced COS7 cells was induced by doxycycline for 2 days, or not; cells were cultured overnight in low serum conditions, and then treated, or not, with serum (10% final foetal bovine serum) for 10 min before to be washed (ice-cold PBS with 0.1 mM orthovanadate) and lysed with the same lysis buffer than for kinase assays and proteins samples were processed by the same method (see above). ERK activation was analysed by western blot with anti phospho-ERK antibodies (T202/Y204, Cell Signaling, #4370), and then sample loading assessed by anti-α tubulin revelation.

To test *α*PIX and *β*PIX binding, HEK cells were cotransfected with the plasmids of interest with Lipofectamine as described above and controls were done with a PAK3 variant bearing the double point mutation (P194G-R195A) in the proline-rich segment known to totally suppress PAK/PIX interaction and with a *β*PIX construct with a deletion of the SH3 domain (ΔSH3). Transfected cells were lysed 36 h later with a modified Robert's lysis buffer containing 0.1% Triton X-100, 10% glycerol, 20 mM Tris-HCl pH 8.0, 137 mM NaCl, 50 mM NaF supplemented with protease and phosphatase inhibitors mixture. After 15 min on ice, lysates were cleared by centrifugation at 10,000 $\times g$ for 15 min. A Bradford protein assay (Biorad) was then performed to measure the protein concentration. TCL were immunoprecipitated overnight at 4 °C using monoclonal anti-HA agarose antibody (Sigma-Aldrich, #A2095). Anti-HA immunocomplexes were then washed four times with lysis buffer (previously described). Protein samples were separated by 10% SDS-PAGE. Immunoblot analysis were performed using anti-β-actin (Santa Cruz, #SC-69879), anti-HA (Cell Signaling Technology, #2367), anti-FLAG (Sigma, #F7425) primary antibodies. Membranes were then incubated using anti-mouse (Biorad, #172-1011) peroxidase-linked secondary antibodies. Membranes were then revealed with Luminata Crescendo (Millipore). Quantification was assessed using a CCD camera (Fusion FX imaging system, Vilber Lourmat) and analysis was performed with ImageJ software. Amounts of co-immunoprecipitated FLAG-PIX proteins, detected and quantified by western blot were expressed relatively to HA-immunoprecipitated PAK3 proteins.

2.7. Cell imaging

COS7-Lv-PAK3 cells were plated at low density on glass coverslips and protein expression was induced with doxycycline during 24 h in half conditions. Cells were fixed with 4% p-formaldehyde for 15 min, washed with PBS and permeabilised with 0.1% Triton X-100 and 0.1% Tween 20 for 15 min at room temperature, then blocked with 0.3% bovine serum albumin (BSA) for 2 h at room temperature before an incubation in 0.1% Tween 20, 0.1% BSA with anti-paxillin (Millipore/Upstate, #05–417) and anti-HA (Roche, #1867423) antibodies overnight at 4 °C. Cells were then washed and incubated for 2 h at room temperature in 0.1% Tween 20, 0.1% BSA with Alexa-568 anti-rat (Molecular Probes, #A11077) and Alexa-488 anti-mouse (Molecular Probews, #A21121) antibodies to label adhesion points and PAK3. Slips were mounted on slides with Fluoromount + Dapi (eBioscience, #00-4959-52), and cells were imaged using a Leica DMI6000B microscope and pictures were double blind analysed with ImageJ software (counting, Feret diameter measurement and colocalization). Paxillin-positive dots corresponding to adhesion points were classified as peripheral focal complexes and as central focal adhesions. The two classes of adhesion points were quantified for each mutant cell line with or without doxycycline induction. Each quantification was then normalized to its own non-induced control. Illustrating images were obtained with a confocal microscope LSM700 (Zeiss, Germany).

2.8. Cell circularity analysis

Protein expression of PAK3 variants was induced with doxycycline during 48 h in half conditions. Then, COS7-Lv-PAK3 cells were plated at low density on glass coverslips and fixed with 4% p-formaldehyde for 15 min after a 5 h period of spreading. Then coverslips were permeabilised and blocked as above and incubated with anti-HA antibody (Roche, #1867423) overnight at 4 °C. Cells were then washed and incubated for 2 h at room temperature in 0.1% Tween 20, 0.1% BSA with Alexa-568 anti-rat antibody (Molecular Probes, #A11077) and Alexa-A488 phalloïdin (Molecular Probes, #A12379) to label PAK3 and F-actin. Slips were mounted on slides with Fluoromount + Dapi (eBioscience, #00–4959-52), and large tile-images at maximum magnification rate (25×) were made using an AxioZoom V16 (Zeiss, Germany). After stitching, pictures were analysed with ImageJ software. The Measure command calculates object circularity as follows: circularity = $4\pi(\text{area}/\text{perimeter}^2)$. A circularity value of 1 indicates a perfect circle. As the value approaches 0, it indicates an increasingly elongated polygon. This circularity index was quantified for each mutant cell line with and without doxycycline induction. Each quantification was then normalized to its own non-induced control.

2.9. Wound healing assay

COS7-Lv-PAK3 cells were plated at 7.10^5 cells/mL as recommended by Ibidi using a culture insert with two wells separated by a 500 μm gap (Ibidi GmbH, #81176). One day after, 50 μM of Cytosine Arabinoside (AraC) was added to each well and 2 μg/mL of doxycycline to half conditions. Twenty-four hour later, insert was removed, and wells were washed twice with PBS and a fresh complete growth medium (described before) with AraC and doxycycline (in induced wells) was added. Pictures were then taken using a Leica DMI6000B microscope at 0, 3 and 5 h after insert withdrawal. Migration analysis was performed with ImageJ software: each induced cell line migration was normalized and compared to its non-induced control.

To quantify cell apoptosis in these conditions, we performed anti-cleaved caspase 3 labelling using the following protocol: cells were fixed with 4% p-formaldehyde for 15 min, washed with PBS and permeabilised/blocked with 5% goat normal serum and 0.3% Triton for 2 h at room temperature before an overnight incubation at 4 °C in PBS with 1% BSA and 0.3% Triton containing rabbit anti-cleaved caspase 3 antibody (Cell Signaling #9664). Cells were then washed and incubated for 2 h:30 in PBS with 1% BSA and 0.3% Triton containing goat anti-rabbit A568 antibody (Mol Probes #A11036). Slips were mounted on slides with Fluoromount + Dapi (eBioscience, #00-4959-52), and cells were imaged using a Leica DMI6000B microscope and pictures were analysed with ImageJ software.

2.10. Statistical analysis

Biochemical experiments (protein stability and protein interaction assay) and wound healing assay were conducted at least three times and data are presented as mean ± SEM. Normal distribution and variance equality were tested with a Shapiro test and Bartlett test. Then, a pairwise *t*-test with a «Benjamini-Hochberg» correction was performed. For cellular adhesion point analysis, experiments were realized at least three times and we performed a pairwise Wilcoxon test with a «Benjamini-Hochberg» correction as data were not following a normal distribution. A p-value of < 0.05 was considered to be significant.

3. Results

3.1. New PAK3 mutation in a family with X-linked CCA

The patient is the second son of healthy and unrelated parents from Maghreb (Fig. 1A). From a first consanguineous union, the mother had a healthy daughter. The mother had one healthy sister and two healthy brothers. The maternal grandmother had two brothers including one with ID who died at 11 years old and one who died at birth. The first pregnancy of the couple was terminated at 34 weeks of gestation after prenatal ultrasound diagnosis of CCA associated with severe hydrocephaly in a male fetus. Neuropathological examination showed that the brain weight was over the 95th centile and confirmed a subtotal CCA with presence of Probst bundles, a septal dysgenesis associated with triventricular dilatation, a massive gliosis of white matter and subependymal cystic lesions. The second pregnancy gave birth to a premature boy who died at birth. During the third pregnancy, CCA was diagnosed by ultrasound. The parents decided to continue the pregnancy and the patient was born eutrophic at 39 weeks of gestation (weight 3595 g, length 47 cm, head circumference 33 cm). The first years of life were characterized by global development delay (the patient walked at 3 years, said his first words at 5 years) and behavior disturbances (including frequent hand stereotypies). At age of 7 years, the patient's weight was 19 kg (− 1 SD), height at 108 cm (− 2 SD) and head circumference at 47 cm (− 3 SD). He had ID and spoke only a few words. At neurological examination, he had contractures of knees and hips with normal tendon reflexes. Brain MRI at the age of 6 years showed a short corpus callosum with global hypoplasia predominating in its posterior part (Fig. 1B). He had no other brain or extra-cerebral malformations. Clinical examinations of the patient over a long period did not reveal any ichthyosis or other cutaneous abnormalities. Karyotyping and microarray of the patient were normal. In search for the etiology, we performed trio-based whole exome sequencing and identified a single nucleotide variation in the *PAK3* gene (ChrX (GRCh37):g.110439731G > A, c.1270G > A in the NM_001128166 transcript, p.Gly424Arg) inherited from his mother. Familial segregation showed that the sibling aborted fetus with hydrocephaly and CCA also carried the mutation at hemizygous state whereas the healthy maternal uncle did not. This mutation is absent from the control subject databases GnomAD, dbSNP, and 1000 Genome and was not found in the clinical database ClinVar (1000 Genomes Project Consortium et al., 2012; Landrum et al., 2018; Sherry et al., 2001). Identified variant was deposited in the ClinVar Database where it is publicly available and can be found with accession number SCV000897773 for c.1270G > A at the following link: https://www.ncbi.nlm.nih.gov/clinvar/variation/626256/.

3.2. The conserved G424 residue forms the hinge of the activation loop of the catalytic domain

The c.1270G > A mutation leads to a non-synonymous change (p.Gly424Arg). This G424 residue is totally conserved among the human PAK paralogous (PAK1/2/4/5/6) and among the other PAK orthologous proteins in vertebrate and invertebrate organisms (Figs. 2A and S1A). This residue is conserved in around half of the human kinome (57%), especially in the AGC and STE kinase families (Fig. S1B). *In silico* prediction analyses indicated that the variant should be disease-causing since Polyphen-2 and SIFT/Provean predicts a damaging effect with any

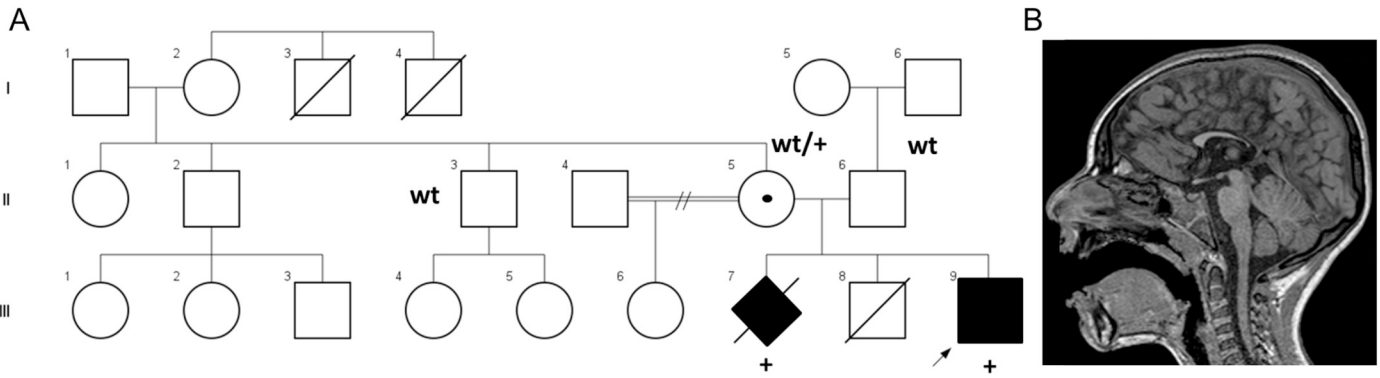

Fig. 1. Genetical and clinical description. (A) Family pedigree of the identified *PAK3* variant c.1270G > A. The variant is at hemizygous state in the patient (III-9) and his sibling fetus (III-7). The mother (II-5) carries this variant at heterozygous state. Familial segregation showed the PAK variant was not carried by a healthy maternal uncle (II-3). (B) Brain MRI of the patient (III-9) at the age of 6 years old showing short corpus callosum with severe splenium hypoplasia.

A

	Species	Protein	aa	Sequence alignment
PAK3	Human WT	PAK3	424	DFGFCAQITPEQSKRSTMV**G**TPYWMAPE
	Human mutant		424	DFGFCAQITPEQSKRSTMV**R**TPYWMAPE
Ort	Drosophilia melanogaster	DmPAK	450	DFDFCANIEGD-EKRQTMV**G**TPYWMAPE
	Caenorhabditis elegans	CePAK	451	DFGDCAQLSPEQRKRTTMV**G**TPYWMAPE
Para	Human	PAK1	426	DFGFCAQITPEQSKRSTMV**G**TPYWMAPE
		PAK2	421	DFGFCAQITPEQSKRSTMV**G**TPYWMAPE
		PAK4	477	DFGFCAQVSKEVPRRKSLV**G**TPYWMAPE
		PAK5	605	DFGFCAQVSKEVPRRKSLV**G**TPYWMAPE
		PAK6	563	DFGFCAQISKDVPKRKSLV**G**TPYWMAPE

B

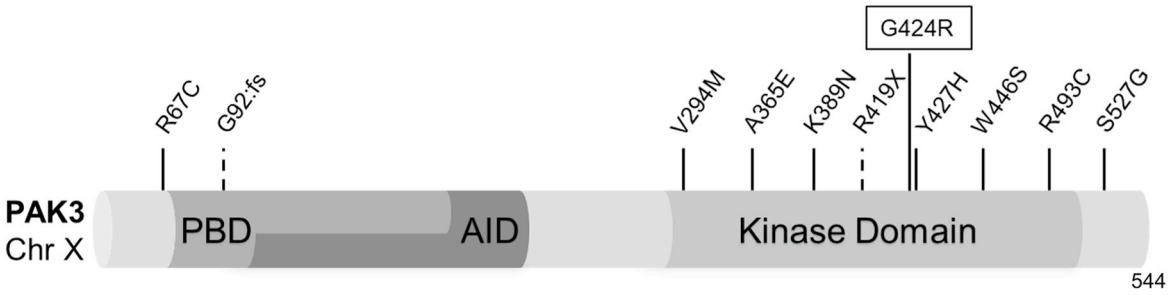

C

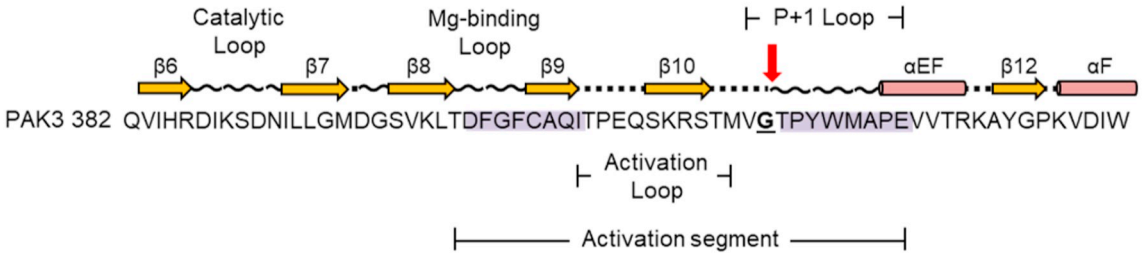

D

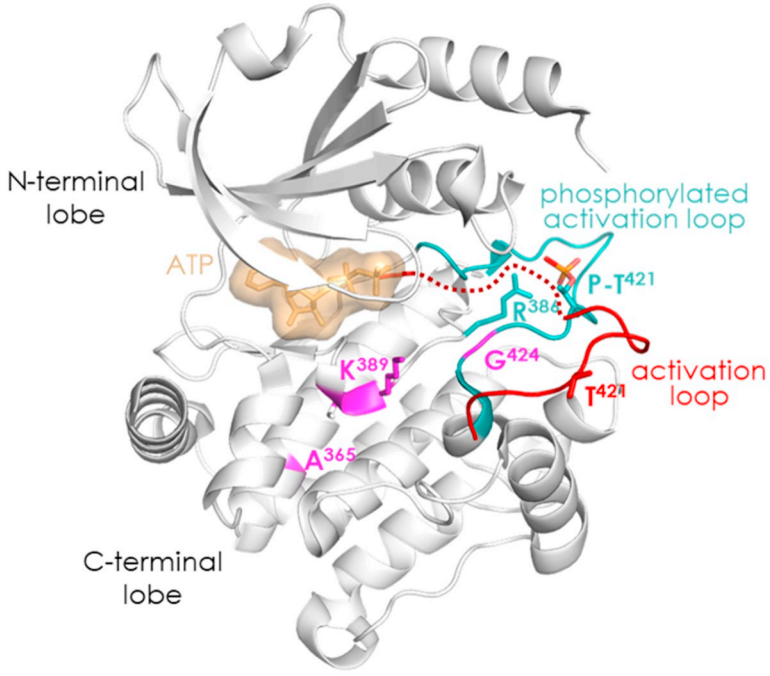

(caption on next page)

Fig. 2. *In silico* analysis of the G424 residue. (A) Sequence alignment of PAK3, orthologous (Ort) and paralogous (Para). Accession numbers for Drosophila and Caenorhabditis orthologous are respectively FBtr0083312 and C09B8.7a. The mutated residue is underlined. (B) Model representing PAK3 protein with previously described mutations and showing functional domains as p21-binding domain (PBD), autoinhibitory domain (AID) and kinase domain. The new G424R mutation is located at the kinase domain. (C) Sequence/structure corresponding of PAK3 protein. Yellow arrows are β-strands and red cylinders are *α*-helices. Red arrow shows the hinge point at the beginning of the p + 1 loop which correspond to the mutated residue (G424R). Purple boxes indicate the anchor points of the activation segment. Adapted from Nolen (Nolen et al., 2004). (D) 3D structure of PAK3 kinase domain depicting the localization of the three mutations in the C-terminal lobe of the catalytic domain (shown in pink). The unphosphorylated inactive conformation of the activation loop is shown in red and the phosphorylated active conformation is shown in green. Ala365 is buried inside the lobe, K389N is located at the tip of the loop that carries Arg386, a residue that is critical for the stabilization of the activation loop, and G424 is located at the hinge of the activation loop. The unphosphorylated activation loop is taken from the structure of unphosphorylated PAK1 and overlaid to phosphorylated PAK3, with residue too flexible to be seen in the crystal structure schematized by a dotted line. fs: frameshift. (For interpretation of the references to colour in this figure legend, the reader is referred to the web version of this article.)

substitution of this residue (Polyphen-2: 1.0; SIFT:0.00 scores) (Adzhubei et al., 2013; Kumar et al., 2009). The G424 residue is located in the kinase domain, like most of the previously described *PAK3* mutations. It is located at the C-terminal hinge between the activation loop (which carries Threonine 421, the main phospho-site involved in PAK3 activation and controls substrate accessibility) and the P + 1 loop in the activation segment (Fig. 2B–D) (Nolen et al., 2004). More precisely, this residue supports the remodeling of the activation loop from its unphosphorylated, inactive conformation (shown in red) to its active, phosphorylated conformation (shown in green), (Fig. 2D). Φ and ψ angles analysis of the two hinge glycine residues of the activation loop shows that the N-ter Gly407 ($\Phi = -73$, $\psi = -11$) is in the "general favoured" region of the Ramachandran plot while the C-ter Gly424 ($\Phi = 132$, $\psi = -160$) is in a "Glycine favoured" region signifying that at the position 424 it can only be a glycine residue (Fig. S2) (Lovell et al., 2003). Thus, mutation to Arg424, a residue that cannot function as a hinge is predicted to impair the conversion of PAK3 to its active conformation without affecting its stability and likely affects the dependent processes from this segment, particularly the kinase activity. The two other mutations included in this study are also located in the kinase domain. Ala365 is buried inside the lobe, where its mutation into a bulkier Glu residue may result into structural misfolding. K389N is located at the tip of the loop that carries Arg386, a residue that is critical for the stabilization of the activation loop by binding to phosphorylated Thr421 in the activation loop. Its mutation to Asn, a residue known to support a wide range of main chain conformations, is likely to alter the stability of PAK3 and/or the conformation of the phosphorylated, active form of the kinase.

3.3. The K389N and G424R mutations abrogate kinase activity without affecting protein stability

Since mutations in the activation segment may have opposite effects, we analysed the effect of the G424R mutation on kinase activity (Dixit and Verkhivker, 2014). We compared the new G424R variant to the two previously described A365E and K389N mutations, which are both located in the kinase domain but lead to differential phenotypes, *i.e.* nonsyndromic mild ID and severe ID associated with CCA, respectively. From this point on, the G424R and K389N variants will be coined as "severe PAK3" mutations (for "associated with severe phenotypes") and the A365E as "mild PAK3" mutation (for "associated with a mild phenotype"). These *PAK3* mutants were transiently co-expressed in HEK cells with constitutively active or dominant negative forms of the CDC42 GTPase. Controls included the WT PAK3 protein and the K297L kinase-dead mutant, generated by disruption of the ATP-binding site of the catalytic domain and recurrently used as control for kinase activity. Upon co-expression with the constitutively active CDC42-V12 mutant, all three immunoprecipitated PAK3 mutant proteins displayed no kinase activity (like the negative control K297L mutant), whereas the WT protein displayed high activity (Fig. 3). The loss of kinase activity may contribute to the pathogenicity of the three mutants but would not explain the different clinical phenotypes associated with them.

As previously suggested by Magini and colleagues, the stability of

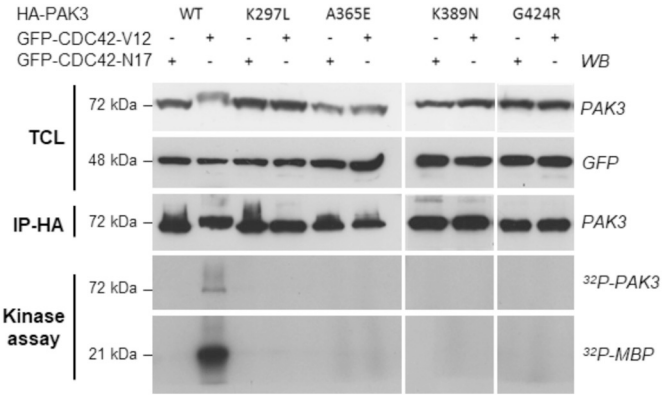

Fig. 3. Kinase activity suppression with the new mutant G424R and other PAK3 mutations. PAK3-WT or mutant proteins were immunoprecipitated after being coexpressed with either dominant-negative (N17) or constitutively active (V12) GFP-CDC42 proteins. Expression levels of transfected proteins were evaluated by western blot, using anti-PAK3 and anti-GFP antibodies (upper panel) on total cell lysate aliquots (TCL). Amount of immunoprecipitated proteins were verified by HA-western blot (IP-HA). Note the electrophoretic shift observed for the WT PAK3 protein coexpressed with V12-CDC42, mainly due to autophosphorylation events. Radioactive phosphorylated MBP and PAK3 proteins were detected by autoradiography (lower panels: kinase assay). These results have been reproduced in three independent experiments. WB: western blot; IP: immunoprecipitation.

mutated PAK3 proteins may in part explain the severity of the disease (Magini et al., 2014). To explore this hypothesis, we tested the degradation time course of these proteins without affecting the biosynthesis of other cellular proteins using a new approach based on the withdrawal of the antibiotic that positively controls the transcription of the gene of interest. We established COS7-Lv-PAK3 cell lines in which *PAK3* expression was induced by doxycycline thanks to a Tet-On expression system (Fig. 4A). HA-PAK3 mutated protein expression was high after 2 days of antibiotic treatment, except for the A365E mutant, and not detectable in absence of doxycycline (Fig. 4B). PAK3 protein stability was monitored by western blot after doxycycline withdrawal. Interestingly, the two K389N and G424R variants displayed a similar stability to those of the WT and the referent kinase-dead K297L proteins (Fig. 4C). Only the A365E mutation destabilized the protein, as previously shown (Magini et al., 2014). This probably explains the low expression level of this mutant, upon doxycycline treatment. Thus, the two severe mutations maintain normal protein stability in contrast to the mild mutation, suggesting that catalytically inactive and stable proteins may induce cell defects by interfering with signalling pathways by protein/protein interaction in addition to the enzymatic loss of function.

3.4. PAK3 mutations associated with CCA affect αPIX binding and cell adhesion dynamics

An alteration of specific protein/protein interactions may characterize some mutation-associated phenotypes (Sahni et al., 2015). The

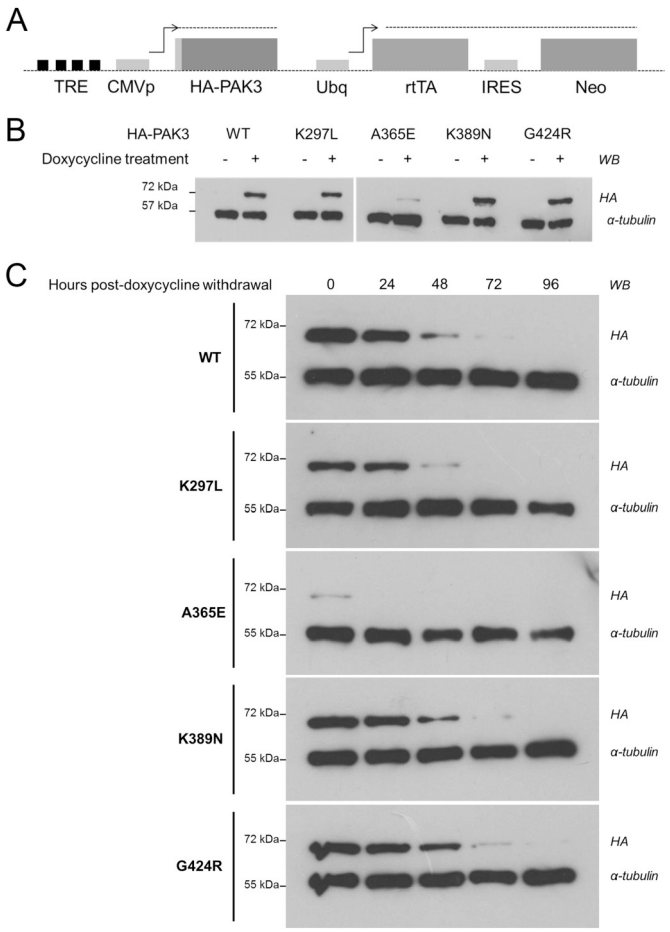

Fig. 4. Severe mutations do not affect PAK3 protein stability. (A) Schematic representation of the Tet-On pHAGE vector containing the Tet-responsive element (TRE), mutant HA-tagged PAK3 coding sequences (HA-PAK3), a transactivator (rtTA), and a gene of selection (Neo). (B) *PAK3* variants are correctly expressed after a 48 h induction period with doxycycline. Anti-HA and anti-α-tubulin antibodies were used to reveal their expressions. Note however that the A365E variant was less detected than other PAK3 proteins. (C) Protein stability was assessed after doxycycline withdrawal and protein expression was analysed by western blot on TCL after 1–4 days of doxycycline withdrawal with anti-HA and anti-*α*-tubulin antibodies. Experiments were independently done three times and data shown are representative of a typical experiment. Ubq: ubiquitin promotor, CMVp: Cytomegalovirus promotor, IRES: Internal Ribosome Entry Site.

main partners of PAK are the *α*PIX and *β*PIX Guanine exchange factors encoded by *ARHGEF6* and *ARHGEF7* genes, respectively (Bokoch, 2003). These GEF play a major role in neuronal signalling and some mutations leading to ID have been identified in the *ARHGEF6* gene (Kutsche et al., 2000). PAK proteins form tight complexes with PIX through an interaction between a non-conventional proline-rich segment of PAK and the PIX SH3 domain allowing their membrane recruitment (Bagrodia et al., 1998; Baird et al., 2005; Manser et al., 1998). We thus analysed the binding of PAK3 variants to *α*PIX and *β*PIX by co-immunoprecipitation assay in transiently transfected HEK cells and western blotting. The absence of co-immunoprecipitation using the P194G-R195A PIX-interacting mutant (PIM) of PAK3 (Fig. 5A and C) and a SH3 deleted *β*PIX construct (data not shown) demonstrated the specificity of this assay. We observed that the amount of PAK3-*α*PIX complexes formed with the K297L and A365E variants did not differ from those formed with the WT protein (WT mean = 0.41; K297L mean = 0.6, p = .37; A365E mean = 0.53, p = .44), whereas the K389N and G424R mutants tended to form more complexes with *α*PIX (WT mean = 0.41; K389N mean = 0.8, p = .056; G424R mean = 0.76, p = .07; Fig. 5A and B). In the same experimental approach, PAK3 mutants and the WT protein formed equal amounts of PAK3/*β*PIX complexes (Fig. 5C and D).

Because the dynamics of adhesion points is regulated by the PAK/PIX pathway, we then analysed the effect of PAK3 variants on the number of adhesion points (Nayal et al., 2006; Zhao et al., 2000). Cell adhesion points were detected by paxillin immunolabeling and quantified in dox-treated COS7-Lv-PAK3 cell lines relative to those observed in untreated cells. We first checked that doxycycline addition had no effect on the number of paxillin-positive adhesion points in non-transduced COS7 cells (Fig. S3B) and that the different expression levels of HA-PAK3-WT (low, medium or high) had no effect on the number of paxillin-positive points per cell (Fig. S3A). This result was also observed for the PAK3 mutants (data not shown). The expression of the WT protein did not change the number of paxillin-positive points compared to non-induced cells as indicated by a ratio around 1 (Fig. 6B). In cells expressing the A365E PAK3 mutation, the total number of paxillin-positive points was not significantly modified whereas the number of peripheral focal complexes was increased compared to WT-expressing cells (WT median = 1; A365E median = 1.2, $p \leq .001$). In contrast, the expression of the severe K389N and G424R PAK3 variants significantly increased the total number of paxillin-positive points per cell (WT median = 0.98; K389N median = 1.27, $p \leq .001$; G424R median = 1.17, $p \leq .01$; Fig. 6B) with an increase of both peripheral focal complexes (WT median = 1; K389N median = 1.3, $p \leq .001$; G424R median = 1.08, $p \leq .05$) and central focal adhesions per cell (WT median = 1; K389N median = 1.8, $p \leq .001$; G424R median = 1.4, $p \leq .01$) compared to WT-expressing cells (Fig. 6C and D). After induction, we also observed an enrichment of the three kinase-dead PAK3 mutants in paxillin-positive points compared to WT condition, as previously reported for the K297L kinase-dead protein (as illustrated on Fig. 6A) (Sells et al., 2000). We conclude that both severe PAK3 mutants affect cell adhesion more severely than the mild A365E mutant.

3.5. Severe PAK3 mutations modify cell spreading and cell migration

While analyzing the effect of PAK3 variants on cell adhesion, we noticed that cells expressing kinase-dead mutants seemed to be more rounded after doxycycline induction in agreement with the role of PAK kinases in cell spreading (Price et al., 1998; Sells et al., 2000). Thus, we analysed in the first 5 h after seeding the cell circularity in non-induced cells and in PAK3 mutants-expressing cells. After fixation, COS7-Lv-PAK3 cells were labeled with fluorescent phalloidin in order to visualize the F-actin network and cell edges (Fig. 7A). We measured cell area, perimeter and circularity that is defined by the two previous parameters. The expression of the three kinase-dead mutants triggered a significant increase in cell circularity (WT median = 0.89; A365E: median = 1.05; K389N: median = 1.28; G424R: median = 1.18; $p \leq .001$ for each mutant; Fig. 7B) and in cell area (WT median = 0.95; A365E: median = 1.08; K389N: median = 1.13; G424R: median = 1.28; $p \leq .001$ for each mutant; Fig. 7C), compared to that of WT PAK3 expressing cells. No significant differences were observed for cell perimeter (data not shown). These results were all the more robust as doxycycline treatment of non-transduced COS7 cells induced a decrease in cells area or circularity (Fig. S3C and S3D) and no effect on cell perimeter (Fig. S3E).

Because adhesion points and cell spreading play a critical role in cell mobility, we analysed the effect of the expression of PAK3 variants on the migration of COS7-Lv-PAK3 cells with a wound healing test. PAK3 expression was induced by addition of doxycycline and proliferation was blocked with antimitotic AraC treatment. The gap relative closure was quantified 3 and 5 h after inserts withdrawal. Expression of the WT PAK3 protein had no significant effect on the gap closure compared to the non-induced cells. In contrast, A365E-expressing cells displayed a 20% reduction of migration observed after 5 h compared to non-

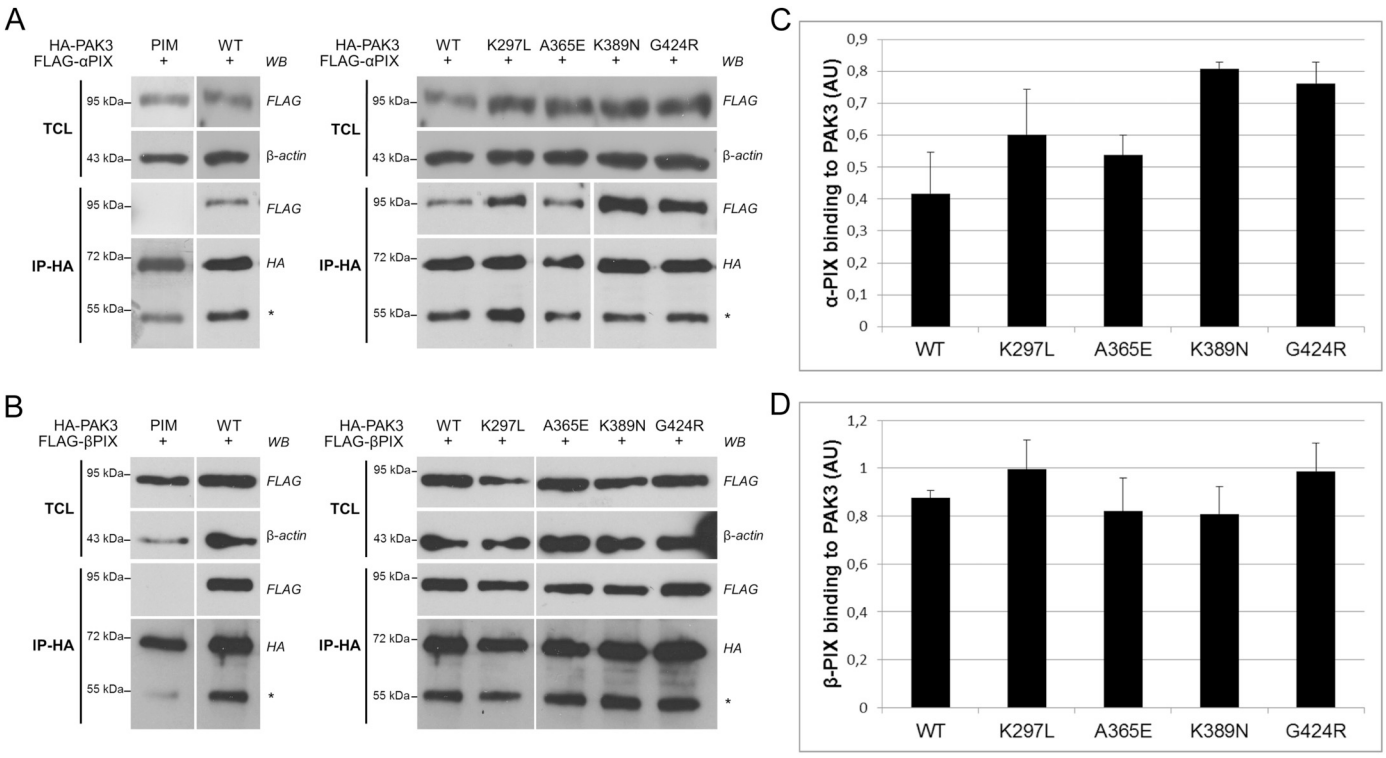

Fig. 5. *α*PIX binding increases with severe PAK3 K389N and G424R mutants. HEK cells were cotransfected with PAK3-WT or mutants, in presence of either *α*PIX or *β*PIX, both FLAG-tagged. A PIX-interacting mutant (PIM) of PAK3 was also used to control specificity of assay. HA-tagged PAK3 proteins were immunoprecipitated and western blots probed with anti-HA, anti-FLAG and anti-β-actin antibodies were performed on TCL and immunoprecipitated samples. Intensities were quantified with a chemiluminescence imager. Co-immunoprecipitated FLAG-PIX proteins were normalized to immunoprecipitated HA-PAK3 protein. Asterisks in western blot correspond to immunoglobulin bands. (A) Representative western blot of *α*PIX binding to PAK3. (B) Interaction quantification for *α*PIX. (C) Representative western blot of *β*PIX binding to PAK3. (D) Interaction quantification for *β*PIX. Results are presented as mean + SEM. $N = 4$.

induced cells whereas the two severe kinase-dead variants K389N and G424R displayed a more drastic decrease of migration from 3 h of 40–60% compared to their own non-induced cells (Fig. 8). We verified that this decrease of migration is not due to an increase of apoptosis, by cleaved-caspase 3 labelling (Fig. S4). Together expression of severely pathogenic PAK3 variants impacted cell migration.

4. Discussion

CCA may be associated with neurodevelopmental disorders, mainly with ID. Hundreds of genetic anomalies (copy number variations and gene mutations) have been identified by chromosomal microarray analyses and next generation sequencing in patients with CCA associated with ID, thereby generating a great nosological and etiological complexity (Edwards et al., 2014; Heide et al., 2017). Moreover, different mutations in a single gene may lead to distinct clinical phenotypes, including ID with and without CCA, which raises the issue of the genotype/phenotype correlation. In the present work, we described a new family with ID and CCA found in several males, which strongly suggested an X-linked disorder. Whole Exome Sequencing allowed us to identify a new mutation in the *PAK3* gene located on the X chromosome. Several *PAK3* mutations have been previously identified in patients with nonsyndromic ID highlighting the role of *PAK3* in synaptic plasticity through a main signalling pathway involving Rho-GTPases of the RAC and CDC42 family and targeting actin dynamics and dendritic spine remodeling (Allen et al., 1998; Bienvenu et al., 2000; Dubos et al., 2012; Gedeon et al., 2003; Kreis and Barnier, 2009; Ramakers, 2002; Rejeb et al., 2008; Sala and Segal, 2014). This pathway also plays a crucial role in brain development since mutations in *RAC1*, *CDC42* and *PAK1* genes were identified in patients with ID and microcephaly or macrocephaly (Harms et al., 2018; Martinelli et al., 2018; Reijnders et al., 2017). However the three PAK isoform seem to have specific and unique neuronal functions since their mutations lead to different symptoms, such as neurodevelopmental delay and microcephaly for PAK1, autism spectrum disorder for PAK2 and ID for PAK3 (Harms et al., 2018; Wang et al., 2018). Interestingly, several *PAK3* mutations were identified in patients with ID and structural brain anomalies (Table 1). Microcephaly was reported in 13/29 individuals in 7 out 11 pedigrees and was associated with distinct mutations. Microcephaly did not correlate with the severity of ID, as illustrated by patients with the V294M variant and those with the R419X variant, both associated with microcephaly and mild ID (Allen et al., 1998; Muthusamy et al., 2017).

Most mutations associated with microcephaly are missense mutations but two patients with the R419X nonsense mutation and two patients with a N-terminal frameshift also display this morphological defect. Concerning kinase activity, it is difficult to conclude that the loss of this function is sufficient to induce microcephaly. Indeed, patients harboring the A365E mutation which totally impairs the PAK3 enzymatic activity do not display microcephaly (Gedeon et al., 2003). Interestingly, one mutation probably responsible for a relative gain of function through a partial activation of its kinase activity is associated with macrocephaly (Hertecant et al., 2017). Concerning the severity of the pathogenicity of some missense mutations compared to nonsense or frame-shift mutations, we propose that the absence of protein has less pathogenic consequences than mutated variant proteins, because missense variants can adversely interfere with signalling pathways. Such hypothesis has already been developed for *PAK3* mutations that impact PAK dimer signalling and MAPK activation (Combeau et al., 2012; Magini et al., 2014).

Anomalies of the corpus callosum were reported in three pedigrees with different *PAK3* missense variants, including our study (Table 1) (Horvath et al., 2018; Magini et al., 2014). However, all patients did not

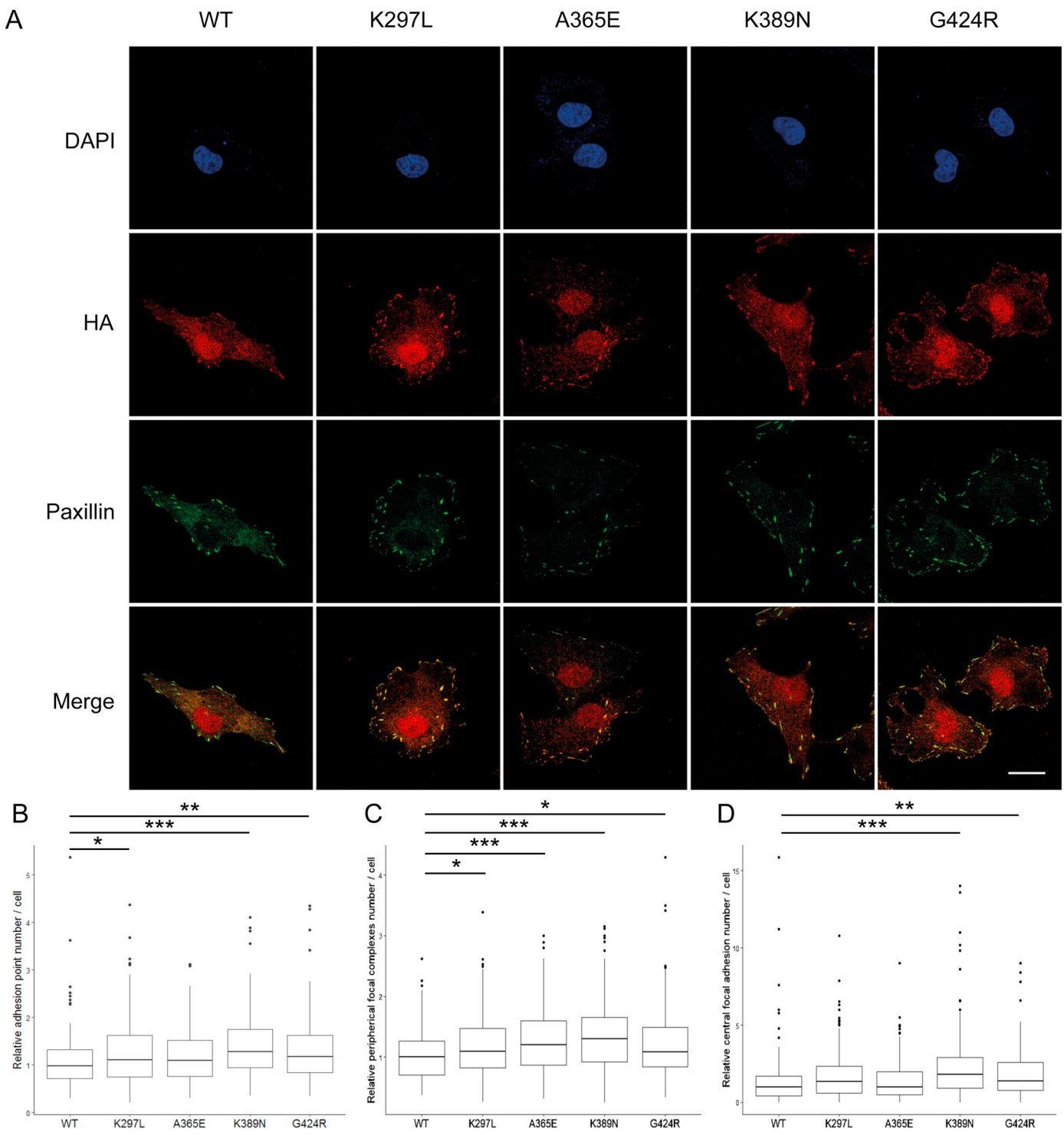

Fig. 6. Kinase dead mutants modify protein localization and severe PAK3 mutants increase cell adhesion point number. PAK3 variant expression was induced in COS7-Lv-PAK3 cell lines during 24 h in presence of doxycycline. (A) Localization of PAK3 proteins. Cells were immuno-stained for HA-PAK3 and endogenous paxillin. Pictures were used to state on the localization of PAK3 which is enriched in cell adhesion points for all the kinase dead mutants. Scale bar = 20 μm. (B) Relative cell adhesion point number per cell. (C) Relative peripheral focal complexes number per cell. (D) Relative central focal adhesion number per cell. Pictures were analysed with ImageJ software in order to quantify cell adhesion point number. Each quantification was normalized to its own non-induced cell control. Three independent experiments have been realized and at least 120 cells were analysed. Data are represented as median and interquartile. Non-parametric tests were used for statistical analysis (*cf.* Material and methods; $^{*}p < 0.05$; $^{**}p < 0.01$; $^{***}p < 0.001$).

undergo brain imaging, thus it is possible that some of the mutations listed in Table 1 may also be associated with CCA. Moreover, the thin corpus callosum described in the patient with the S527G variant may be a secondary cerebral atrophy induced by self-injuries (Horvath et al., 2018). Thus, to date, only the K389N and G424R missense variants located in the catalytic domain and co-segregating with CCA in all individuals disrupt corpus callosum morphogenesis. Corpus callosum abnormalities are caused by developmental defects affecting neuronal proliferation and specification, cell migration and midline patterning, as well as by defects in axonal growth and guidance (Edwards et al.,

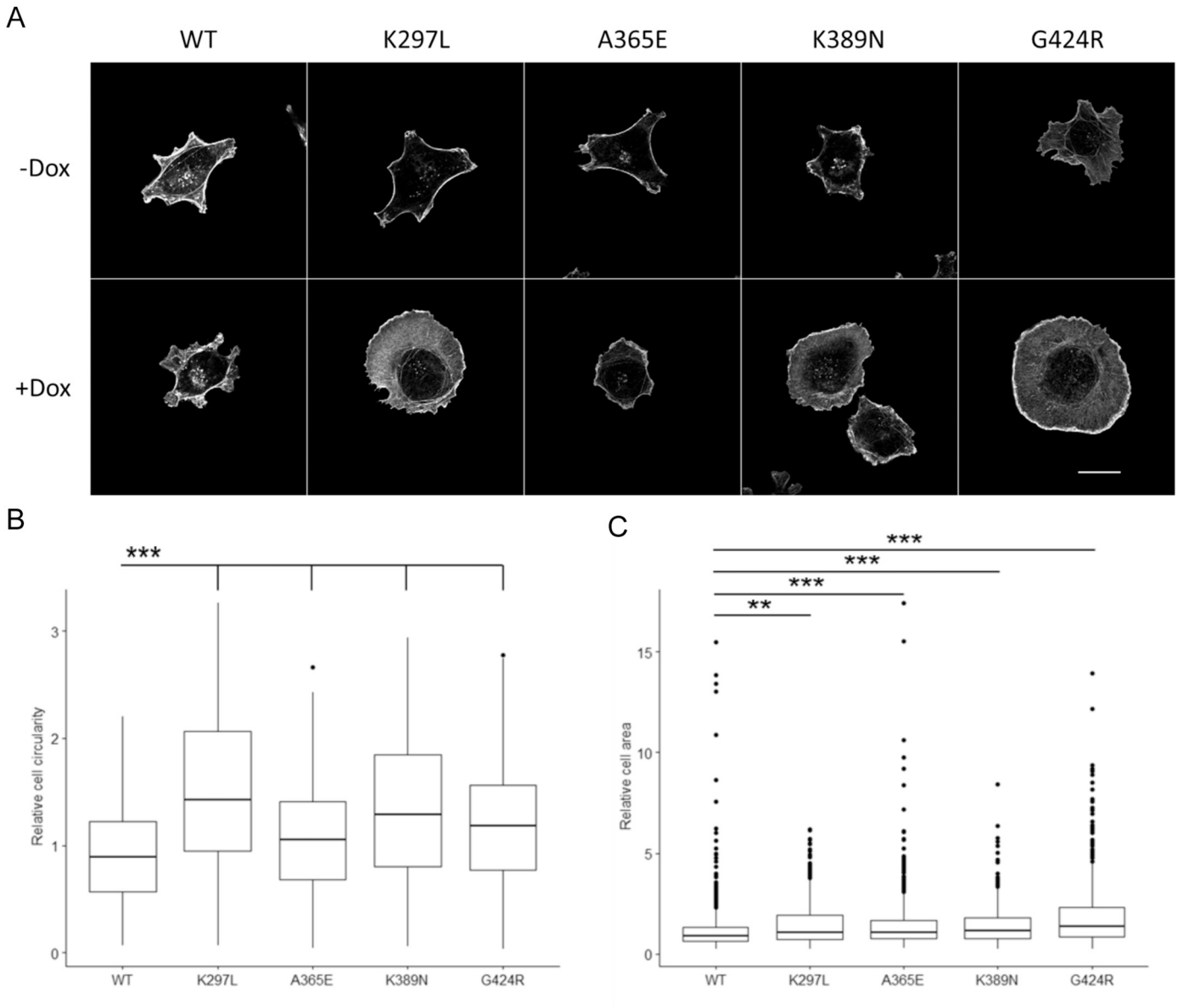

Fig. 7. Kinase dead mutants lead to more rounded and spread cells. PAK3 variants expression was induced in COS7-Lv-PAK3 cell lines during 48 h in presence of doxycycline. Cells were plated and then fixed 5 h later for phalloidin labeling. Cell circularity was then quantified with ImageJ software. (A) COS7 cells expressing either the WT or the different variants labeled with phalloidin. Scale bar = 20 μm. (B) Relative cell circularity quantification. (C) Relative cell area quantification. Data are represented as median and interquartile, and three independent experiments were realized. Non-parametric tests were used for statistical analysis; (*cf.* Material and methods; $^{*}p < 0.05$; $^{**}p < 0.01$; $^{***}p < 0.001$).

2014). It is well characterized that PAK kinases regulate several of these cellular processes, and more specifically that the *PAK3* isoform controls neuroblast migration and axonal growth (Cobos et al., 2007; Kreis and Barnier, 2009; Liu et al., 2019). To decipher biological processes underlying the phenotypical variability of *PAK3*-associated neurodevelopmental disorders, we compared the effects of the two K389N and G424R mutations associated with severe ID and CCA with the A365E *PAK3* mutation previously reported in patients at the other edge of the clinical spectrum, *i.e.* with mild nonsyndromic ID. We observed no correlation between the loss of kinase activity and the severity of the phenotype. This is in line with the severity of ID ranging from mild in patients with the A365E and W446S mutations that totally suppress the kinase activity to moderate or severe in those with the R67C mutation which retains it (Bienvenu et al., 2000; Gedeon et al., 2003; Peippo et al., 2007; Kreis et al., 2007; Magini et al., 2014).

The G424R mutation is the second identified disease-causing mutation of the PAK3 kinase located in the activation segment, with the previously described Y427H mutation (Hertecant et al., 2017). A major determinant of the regulation of PAK and other kinases is the presence of an activation loop in the C-terminal lobe, which needs to be phosphorylated so that the active site can bind the substrate protein in a productive way. Phosphorylation results in the stabilization of this loop through electrostatic interactions between the phosphorylated threonine and an arginine of the C-terminal domain, and this involves a lasso movement of this loop whose hinges are glycine located at its two ends, one of which is Gly424. As we demonstrated, mutation of this residue totally suppresses the kinase activity, which can be explained by the inability of the activation loop of this mutant to adopt its active conformation. This mutation is thus anticipated to affect the structure and biochemistry of PAK3 in a different manner from other mutations of the catalytic domain involved in intellectual disabilities.

It was previously suggested that the stability of mutated PAK3 proteins may explain the severity of the associated phenotypes. We demonstrated that the A365E variant is unstable, a characteristic that

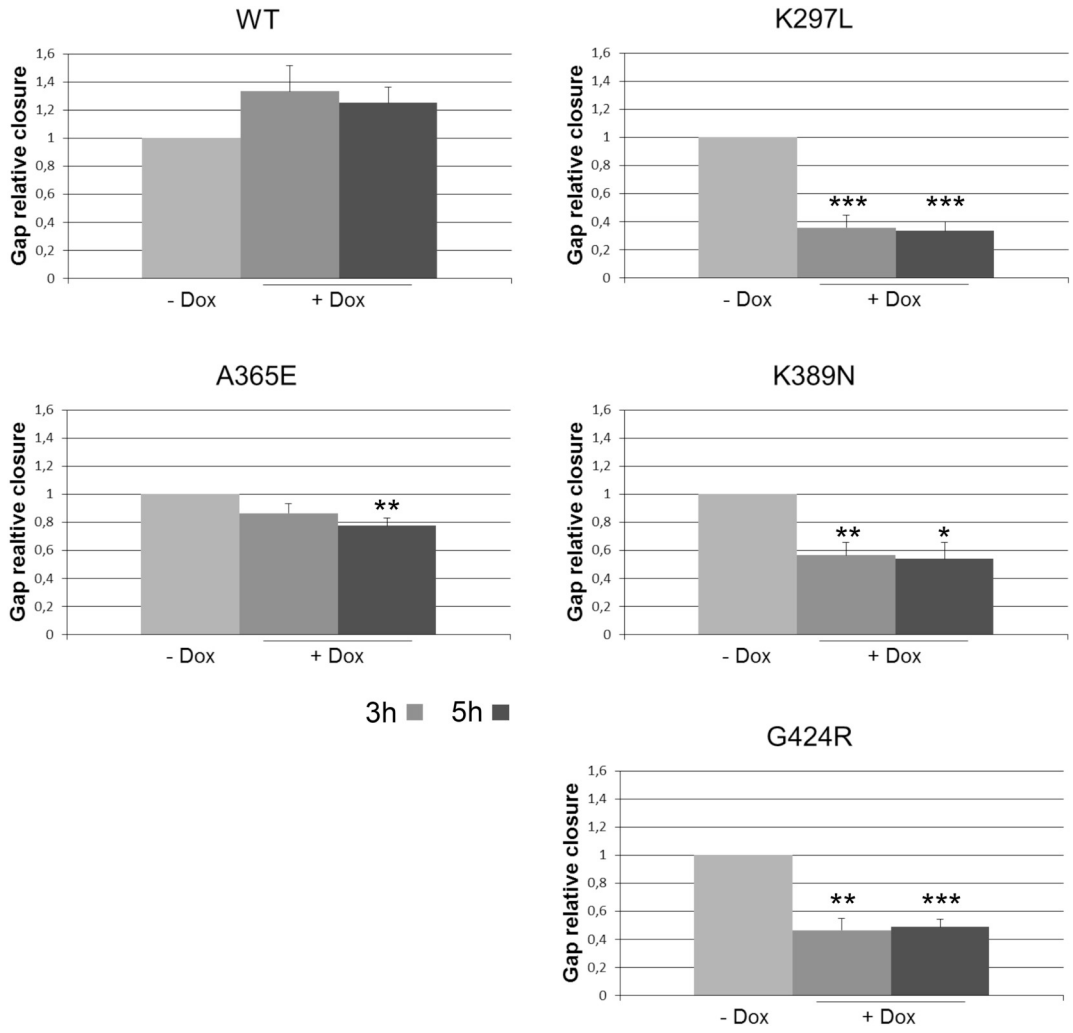

Fig. 8. Severe PAK3 variants K389N and G424R affect cell migration. Expression of PAK3 variants was induced in COS7-Lv-PAK3 cell lines during 24 h in presence of doxycycline. Cell culture was performed using a migration insert and cells were then imaged at 0, 3 and 5 h after insert withdrawal. Gap closure for each mutant was normalized to its own control (non-induced cells). Three independent experiments were performed in duplicate and graphics represent the mean ± SEM. Parametric tests were used for statistical analysis after normality and variance equality verification; ($^{*}p < 0.05$; $^{**}p < 0.01$; $^{***}p < 0.001$).

was previously reported by Magini et al. (Magini et al., 2014). This is readily explained by its buried location, where mutation to a bulkier residue should alter folding of the C-terminal lobe of the kinase domain. In contrast, the K389N and G424R variants display normal stability compared to the WT protein, which may exacerbate their functional consequences by forming inactive complexes with partners. Again, this is consistent with their location at the surface of the kinase domain where they are not expected to impact significantly the stability of the protein (Sorrell et al., 2019). Another non-exclusive hypothesis is that the G424R mutation may modify protein/protein interactions affecting signalling pathways.

PIX proteins are the main partners of group I PAK kinases and form

Table 1
Summary of brain anomalies and intellectual defects of patients with *PAK3* mutations.

Mutants	ID	Number of patients	Microcephaly	Macrocephaly	Callosal anomalies	Reference
R67C	Moderate/severe	6	0/6	0/6	NR	Bienvenu et al. (2000)
G92-fs	Mild	4	2/2	0/2	NR	Rejeb et al. (2008)
V294M	Mild	3	3/3	0/3	NR	Muthusamy et al. (2017)
A365E	Mild	13	0/13	0/13	NR	Gedeon et al. (2003)
K389N	Severe	3	2/3	0/3	3/3	Magini et al. (2014)
R419X	Mild	4	2/4	0/4	0/4	Allen et al. (1998)
G424R	Severe	2	1/2	0/2	2/2	This study
Y427H	Severe	2	0/2	2/2	0/2	Hertecant et al. (2017)
W446S	Mild	5	2/5[a]	0/5	0/3; NR: 2/5	Peippo et al. (2007)
S527G	Mild	1	1/1	0/1	1/1	Horvath et al. (2018)
Deletion	Mild	1	0/1	0/1	NR	Cartwright et al. (2017)

The number of affected patients relative to the total number of examined people was reported: Macrocephaly, microcephaly and corpus callosum (CC) abnormality were indicated. The symptoms of the patient harboring the R493C mutation were not described. NR: not reported.

[a] Head circumference is −2.5 SD below the mean.

supramolecular complexes with GIT proteins, and this complex plays a central role in neuronal signalling by regulating cell adhesion as well as migration, neurite extensions, and synaptic plasticity (Za et al., 2006). Mutations of the αPIX gene located on the X chromosome are also responsible for ID (Kutsche et al., 2000). The regulation of PAK-PIX complexes involves the dimerization of PIXs, their phosphorylation and the combinatory of splice variants (Zhou et al., 2016). Thus, activity-dependent autophosphorylation regulates formation of the PAK/PIX complexes so that kinase-dead mutants form more complexes than WT proteins (Feng et al., 2004). By studying PAK3/PIXs interactions, we observed that the two *PAK3* mutations inducing severe phenotypes tend to enhance PAK3 variant binding to αPIX and that their expression significantly increases the number of cell adhesion points suggesting abnormal turnover of adhesions. Adhesion point and integrin signalling are main regulators of cell migration which is often affected in CCA (Edwards et al., 2014; Zhou et al., 2016). Further experiments showed that the expression of both K389N and G424R mutants strongly modified cell spreading and inhibited the cell migration tested in a wound healing assay. In *PAK3* knock-out mice, it was observed that absence of PAK3 protein did not modify oligodendrocyte progenitor (OPC) migration (Maglorius Renkilaraj et al., 2017). While this may reflect differential molecular mechanisms of migration in these cell types, it is likely that missense mutations affect signalling in a different manner than the absence of the protein, for example by exerting dominant-negative or up-regulated effects. Altogether, these results suggest that mutations that might affect PAK3-PIX signalling may affect cell migration triggering brain morphological anomalies. Further studies with knock-in mouse model could bring a better comprehension of PIX function in pathophysiological mechanisms.

It is remarkable that although the missense K389N and G424R mutations are both expected to affect the kinase activity of PAK3, they display differences at both the clinical and cellular level. At the clinical level, ichthyosis is only diagnosed with the K389N variant whereas clinical traits such as ID, microcephaly, and ACC are observed with both *PAK3* mutations. Likewise, the K389N mutation was shown to impair the MAP kinase pathway, which was proposed to occur through a kinase-independent pathway (Magini), while the G424R mutation has no effect on this pathway (Fig. S5). Links between *PAK3* mutations and MAP kinase activation are complex and may involve both direct and indirect pathways, among which the PAK-PIX axis (Stockton et al., 2007), and that these pathways are differentially affected by PAK3 mutations with different biochemical defects. Notably, the two mutations affect different determinants of the catalytic machinery, with K389N being located in the catalytic site and G424R in the activation loop. We conclude that several pathways such as MAP kinase and/or PIX pathways may be involved in the wide clinical spectrum associated with *PAK3* variants.

In conclusion, our data bring important insight into a cellular mechanism possibly linking *PAK3* mutations to brain dysgenesis. Remarkably, they highlight a remarkable correlation between structural and biochemical defects induced by each mutation to the severity of the associated intellectual disorders. This study also depicts the complexity of the relationship between genotype and phenotype, and strongly suggests that the patient phenotype may be due to the addition of synaptic dysfunctions and developmental defects and may be generated by the sum of biochemical defects such as kinase impairment, protein stability and partner-binding anomalies.

Funding

This work was supported by the french Fondation Jérôme Lejeune [grant number 1705-BJ2017B]; and the french Fondation pour la Recherche Médicale (grant number DEQ20150331694).

Declaration of competing interest

The authors declare that there is no conflict of interest that could be perceived as prejudicing the impartiality of the research reported.

Acknowledgements

We thank the family members for their participation in this study. We thank Emmanuel Thévenot, Nicolas Vitale, Kerstin Kutsche, and Célio Pouponnot for providing us with PAK3- PIM, β-PIX, α-Pix, and replicative lentiviral plasmids, respectively. pHAGE TRE dCas9-VP64 was a gift from Rene Maehr & Scot Wolfe (Addgene plasmid # 50916). We also want to thank the Fondation Jérôme Lejeune for supporting us (JVB) financially and the Fondation pour la Recherche Médicale for supporting JC.

Data availability statement

The data that support the findings of this study are openly available in ClinVar at https://www.ncbi.nlm.nih.gov/clinvar/variation/626256/, reference number SCV000897773.

References

Adzhubei, I., Jordan, D.M., Sunyaev, S.R., 2013. Predicting functional effect of human missense mutations using PolyPhen-2. Curr Protoc Hum Genet Chapter 7, Unit7.20. Curr. Protoc. Hum. Genet. https://doi.org/10.1002/0471142905.hg0720s76.

Allen, K.M., Gleeson, J.G., Bagrodia, S., Partington, M.W., MacMillan, J.C., Cerione, R.A., Mulley, J.C., Walsh, C.A., 1998. PAK3 mutation in nonsyndromic X-linked mental retardation. Nat. Genet. 20, 25–30. https://doi.org/10.1038/1675.

Bagrodia, S., Jordon, K.A., Aelst, L.V., Cerione, R.A., 1998. A novel regulator of p21-activated kinases. J. Biol. Chem. 273, 23633–23636. https://doi.org/10.1074/jbc.273.37.23633.

Baird, D., Feng, Q., Cerione, R.A., 2005. The Cool-2/α-pix protein mediates a Cdc42-Rac signaling cascade. Curr. Biol. 15, 1–10. https://doi.org/10.1016/j.cub.2004.12.040.

Bienvenu, T., des Portes, V., McDonell, N., Carrié, A., Zemni, R., Couvert, P., Ropers, H.H., Moraine, C., van Bokhoven, H., Fryns, J.P., Allen, K., Walsh, C.A., Boué, J., Kahn, A., Chelly, J., Beldjord, C., 2000. Missense mutation in PAK3, R67C, causes X-linked nonspecific mental retardation. Am. J. Med. Genet. 93, 294–298.

Bokoch, G.M., 2003. Biology of the p21-activated kinases. Annu. Rev. Biochem. 72, 743–781. https://doi.org/10.1146/annurev.biochem.72.121801.161742.

Cartwright, A., Smith, K., Balasubramanian, M., 2017. Short case report: Xq23 deletion involving PAK3 as a novel cause of developmental delay in a 6-year-old boy. Clin. Dysmorphol. 26, 38–40. https://doi.org/10.1097/MCD.0000000000000154.

Cobos, I., Borello, U., Rubenstein, J.L.R., 2007. Dlx transcription factors promote migration through repression of axon and dendrite growth. Neuron 54, 873–888. https://doi.org/10.1016/j.neuron.2007.05.024.

Combeau, G., Kreis, P., Domenichini, F., Amar, M., Fossier, P., Rousseau, V., Barnier, J.-V., 2012. The p21-activated kinase PAK3 forms heterodimers with PAK1 in brain implementing trans-regulation of PAK3 activity. J. Biol. Chem. 287, 30084–30096. https://doi.org/10.1074/jbc.M112.355073.

Dixit, A., Verkhivker, G.M., 2014. Structure-functional prediction and analysis of cancer mutation effects in protein kinases. Comput. Math. Methods Med. 2014, 1–24. https://doi.org/10.1155/2014/653487.

Dubos, A., Combeau, G., Bernardinelli, Y., Barnier, J.-V., Hartley, O., Gaertner, H., Boda, B., Muller, D., 2012. Alteration of synaptic network dynamics by the intellectual disability protein PAK3. J. Neurosci. 32, 519–527. https://doi.org/10.1523/JNEUROSCI.3252-11.2012.

Edwards, T.J., Sherr, E.H., Barkovich, A.J., Richards, L.J., 2014. Clinical, genetic and imaging findings identify new causes for corpus callosum development syndromes. Brain 137, 1579–1613. https://doi.org/10.1093/brain/awt358.

Feng, Q., Baird, D., Cerione, R.A., 2004. Novel regulatory mechanisms for the Dbl family guanine nucleotide exchange factor Cool-2/α-Pix. EMBO J. 23, 3492–3504. https://doi.org/10.1038/sj.emboj.7600331.

Gedeon, A.K., Nelson, J., Gécz, J., Mulley, J.C., 2003. X-linked mild non-syndromic mental retardation with neuropsychiatric problems and the missense mutation A365E in PAK3. Am. J. Med. Genet. A 120A, 509–517. https://doi.org/10.1002/ajmg.a.20131.

Genomes Project Consortium, Abecasis, G.R., Auton, A., Brooks, L.D., DePristo, M.A., Durbin, R.M., Handsaker, R.E., Kang, H.M., Marth, G.T., McVean, G.A., 2012. An integrated map of genetic variation from 1,092 human genomes. Nature 491, 56–65. https://doi.org/10.1038/nature11632.

Grogono, J.L., 1968. Children with agenesis of the corpus callosum. Dev. Med. Child Neurol. 10, 613–616.

Harms, F.L., Kloth, K., Bley, A., Denecke, J., Santer, R., Lessel, D., Hempel, M., Kutsche, K., 2018. Activating mutations in PAK1, encoding p21-activated kinase 1, cause a neurodevelopmental disorder. Am. J. Hum. Genet. 103, 579–591. https://doi.org/10.1016/j.ajhg.2018.09.005.

Heide, S., Keren, B., Billette de Villemeur, T., Chantot-Bastaraud, S., Depienne, C., Nava, C., Mignot, C., Jacquette, A., Fonteneau, E., Lejeune, E., Mach, C., Marey, I., Whalen, S., Lacombe, D., Naudion, S., Rooryck, C., Toutain, A., Caignec, C.L., Haye, D.,

Olivier-Faivre, L., Masurel-Paulet, A., Thauvin-Robinet, C., Lesne, F., Faudet, A., Ville, D., des Portes, V., Sanlaville, D., Siffroi, J.-P., Moutard, M.-L., Héron, D., 2017. Copy number variations found in patients with a corpus callosum abnormality and intellectual disability. J. Pediatr. 185https://doi.org/10.1016/j.jpeds.2017.02.023. 160–166.e1.

Hertecant, J., Komara, M., Nagi, A., Al-Zaabi, O., Fathallah, W., Cui, H., Yang, Y., Eng, C.M., Al Sorkhy, M., Ghattas, M.A., Al-Gazali, L., Ali, B.R., 2017. A de novo mutation in the X-linked PAK3 gene is the underlying cause of intellectual disability and macrocephaly in monozygotic twins. Eur. J. Med. Genet. 60, 212–216. https://doi.org/10.1016/j.ejmg.2017.01.004.

Horvath, G.A., Tarailo-Graovac, M., Bartel, T., Race, S., Van Allen, M.I., Blydt-Hansen, I., Ross, C.J., Wasserman, W.W., Connolly, M.B., van Karnebeek, C.D.M., 2018. Improvement of self-injury with dopamine and serotonin replacement therapy in a patient with a hemizygous PAK3 mutation: a new therapeutic strategy for neuropsychiatric features of an intellectual disability syndrome. J. Child Neurol. 33, 106–113. https://doi.org/10.1177/0883073817740443.

Kreis, P., Barnier, J.-V., 2009. PAK signalling in neuronal physiology. Cell. Signal. 21, 384–393. https://doi.org/10.1016/j.cellsig.2008.11.001.

Kreis, P., Thévenot, E., Rousseau, V., Boda, B., Muller, D., Barnier, J.-V., 2007. The p21-activated kinase 3 implicated in mental retardation regulates spine morphogenesis through a Cdc42-dependent pathway. J. Biol. Chem. 282, 21497–21506. https://doi.org/10.1074/jbc.M703298200.

Kumar, P., Henikoff, S., Ng, P.C., 2009. Predicting the effects of coding non-synonymous variants on protein function using the SIFT algorithm. Nat. Protoc. 4, 1073–1081. https://doi.org/10.1038/nprot.2009.86.

Kutsche, K., Yntema, H., Brandt, A., Jantke, I., Gerd Nothwang, H., Orth, U., Boavida, M.G., David, D., Chelly, J., Fryns, J.-P., Moraine, C., Ropers, H.-H., Hamel, B.C.J., van Bokhoven, H., Gal, A., 2000. Mutations in ARHGEF6, encoding a guanine nucleotide exchange factor for Rho GTPases, in patients with X-linked mental retardation. Nat. Genet. 26, 247–250. https://doi.org/10.1038/80002.

Landrum, M.J., Lee, J.M., Benson, M., Brown, G.R., Chao, C., Chitipiralla, S., Gu, B., Hart, J., Hoffman, D., Jang, W., Karapetyan, K., Katz, K., Liu, C., Maddipatla, Z., Malheiro, A., McDaniel, K., Ovetsky, M., Riley, G., Zhou, G., Holmes, J.B., Kattman, B.L., Maglott, D.R., 2018. ClinVar: improving access to variant interpretations and supporting evidence. Nucleic Acids Res. 46, D1062–D1067. https://doi.org/10.1093/nar/gkx1153.

Liu, J., Liu, Y., Shao, J., Li, Y., Qin, L., Shen, H., Xie, Y., Xia, W., Gao, W.-Q., 2019. Zeb1 is important for proper cleavage plane orientation of dividing progenitors and neuronal migration in the mouse neocortex. Cell Death Differ. https://doi.org/10.1038/s41418-019-0314-9.

Lovell, S.C., Davis, I.W., Arendall, W.B., de Bakker, P.I.W., Word, J.M., Prisant, M.G., Richardson, J.S., Richardson, D.C., 2003. Structure validation by Calpha geometry: phi,psi and Cbeta deviation. Proteins 50, 437–450. https://doi.org/10.1002/prot.10286.

Magini, P., Pippucci, T., Tsai, I.-C., Coppola, S., Stellacci, E., Bartoletti-Stella, A., Turchetti, D., Graziano, C., Cenacchi, G., Neri, I., Cordelli, D.M., Marchiani, V., Bergamaschi, R., Gasparre, G., Neri, G., Mazzanti, L., Patrizi, A., Franzoni, E., Romeo, G., Bordo, D., Tartaglia, M., Katsanis, N., Seri, M., 2014. A mutation in PAK3 with a dual molecular effect deregulates the RAS/MAPK pathway and drives an X-linked syndromic phenotype. Hum. Mol. Genet. 23, 3607–3617. https://doi.org/10.1093/hmg/ddu070.

Maglorius Renkilaraj, M.R.L., Baudouin, L., Wells, C.M., Doulazmi, M., Wehrlé, R., Cannaya, V., Bachelin, C., Barnier, J.-V., Jia, Z., Nait Oumesmar, B., Dusart, I., Bouslama-Oueghlani, L., 2017. The intellectual disability protein PAK3 regulates oligodendrocyte precursor cell differentiation. Neurobiol. Dis. 98, 137–148. https://doi.org/10.1016/j.nbd.2016.12.004.

Manser, E., Loo, T.-H., Koh, C.-G., Zhao, Z.-S., Chen, X.-Q., Tan, L., Tan, I., Leung, T., Lim, L., 1998. PAK kinases are directly coupled to the PIX family of nucleotide exchange factors. Mol. Cell 1, 183–192. https://doi.org/10.1016/S1097-2765(00)80019-2.

Martinelli, S., Krumbach, O.H.F., Pantaleoni, F., Coppola, S., Amin, E., Pannone, L., Nouri, K., Farina, L., Dvorsky, R., Lepri, F., Buchholzer, M., Konopatzki, R., Walsh, L., Payne, K., Pierpont, M.E., Vergano, S.S., Langley, K.G., Larsen, D., Farwell, K.D., Tang, S., Mroske, C., Gallotta, I., Di Schiavi, E., della Monica, M., Lugli, L., Rossi, C., Seri, M., Cocchi, G., Henderson, L., Baskin, B., Alders, M., Mendoza-Londono, R., Dupuis, L., Nickerson, D.A., Chong, J.X., Meeks, N., Brown, K., Causey, T., Cho, M.T., Demuth, S., Digilio, M.C., Gelb, B.D., Bamshad, M.J., Zenker, M., Ahmadian, M.R., Hennekam, R.C., Tartaglia, M., Mirzaa, G.M., 2018. Functional dysregulation of CDC42 causes diverse developmental phenotypes. Am. J. Hum. Genet. 102, 309–320. https://doi.org/10.1016/j.ajhg.2017.12.015.

McMichael, G., Bainbridge, M.N., Haan, E., Corbett, M., Gardner, A., Thompson, S., van Bon, B.W.M., van Eyk, C.L., Broadbent, J., Reynolds, C., O'Callaghan, M.E., Nguyen, L.S., Adelson, D.L., Russo, R., Jhangiani, S., Doddapaneni, H., Muzny, D.M., Gibbs, R.A., Gecz, J., MacLennan, A.H., 2015. Whole-exome sequencing points to considerable genetic heterogeneity of cerebral palsy. Mol. Psychiatry 20, 176–182. https://doi.org/10.1038/mp.2014.189.

Murphy, G.J., Mostoslavsky, G., Kotton, D.N., Mulligan, R.C., 2006. Exogenous control of mammalian gene expression via modulation of translational termination. Nat. Med. 12, 1093–1099. https://doi.org/10.1038/nm1376.

Muthusamy, B., Selvan, L.D.N., Nguyen, T.T., Manoj, J., Stawiski, E.W., Jaiswal, B.S., Wang, W., Raja, R., Ramprasad, V.L., Gupta, R., Murugan, S., Kadandale, J.S., Prasad, T.S.K., Reddy, K., Peterson, A., Pandey, A., Seshagiri, S., Girimaji, S.C., Gowda, H., 2017. Next-generation sequencing reveals novel mutations in X-linked intellectual disability. OMICS 21, 295–303. https://doi.org/10.1089/omi.2017.0009.

Nayal, A., Webb, D.J., Brown, C.M., Schaefer, E.M., Vicente-Manzanares, M., Horwitz, A.R., 2006. Paxillin phosphorylation at Ser273 localizes a GIT1–PIX–PAK complex and regulates adhesion and protrusion dynamics. J. Cell Biol. 173, 587–589. https://doi.org/10.1083/jcb.200509075.

Nolen, B., Taylor, S., Ghosh, G., 2004. Regulation of protein kinases; controlling activity through activation segment conformation. Mol. Cell 15, 661–675. https://doi.org/10.1016/j.molcel.2004.08.024.

Palmer, E.E., Mowat, D., 2014. Agenesis of the corpus callosum: a clinical approach to diagnosis. Am. J. Med. Genet. C: Semin. Med. Genet. 166C, 184–197. https://doi.org/10.1002/ajmg.c.31405.

Peippo, M., Koivisto, A.M., Särkämö, T., Sipponen, M., von Koskull, H., Ylisaukko-oja, T., Rehnström, K., Froyen, G., Ignatius, J., Järvelä, I., 2007. PAK3 related mental disability: further characterization of the phenotype. Am. J. Med. Genet. A 143A, 2406–2416. https://doi.org/10.1002/ajmg.a.31956.

Price, L.S., Leng, J., Schwartz, M.A., Bokoch, G.M., 1998. Activation of Rac and Cdc42 by integrins mediates cell spreading. Mol. Biol. Cell 9, 1863–1871.

Ramakers, G.J.A., 2002. Rho proteins, mental retardation and the cellular basis of cognition. Trends Neurosci. 25, 191–199.

Reijnders, M.R.F., Ansor, N.M., Kousi, M., Yue, W.W., Tan, P.L., Clarkson, K., Clayton-Smith, J., Corning, K., Jones, J.R., Lam, W.W.K., Mancini, G.M.S., Marcelis, C., Mohammed, S., Pfundt, R., Roifman, M., Cohn, R., Chitayat, D., Deciphering Developmental Disorders Study, Millard, T.H., Katsanis, N., Brunner, H.G., Banka, S., 2017. RAC1 missense mutations in developmental disorders with diverse phenotypes. Am. J. Hum. Genet. 101, 466–477. https://doi.org/10.1016/j.ajhg.2017.08.007.

Rejeb, I., Saillour, Y., Castelnau, L., Julien, C., Bienvenu, T., Taga, P., Chaabouni, H., Chelly, J., Jemaa, L.B., Bahi-Buisson, N., 2008. A novel splice mutation in PAK3 gene underlying mental retardation with neuropsychiatric features. Eur. J. Hum. Genet. 16, 1358–1363. https://doi.org/10.1038/ejhg.2008.103.

Rousseau, V., Goupille, O., Morin, N., Barnier, J.-V., 2003. A new constitutively active brain PAK3 isoform displays modified specificities toward Rac and Cdc42 GTPases. J. Biol. Chem. 278, 3912–3920. https://doi.org/10.1074/jbc.M207251200.

Sahni, N., Yi, S., Taipale, M., Fuxman Bass, J.I., Coulombe-Huntington, J., Yang, F., Peng, J., Weile, J., Karras, G.I., Wang, Y., Kovács, I.A., Kamburov, A., Krykbaeva, I., Lam, M.H., Tucker, G., Khurana, V., Sharma, A., Liu, Y.-Y., Yachie, N., Zhong, Q., Shen, Y., Palagi, A., San-Miguel, A., Fan, C., Balcha, D., Dricot, A., Jordan, D.M., Walsh, J.M., Shah, A.A., Yang, X., Stoyanova, A.K., Leighton, A., Calderwood, M.A., Jacob, Y., Cusick, M.E., Salehi-Ashtiani, K., Whitesell, L.J., Sunyaev, S., Berger, B., Barabási, A.-L., Charloteaux, B., Hill, D.E., Hao, T., Roth, F.P., Xia, Y., Walhout, A.J.M., Lindquist, S., Vidal, M., 2015. Widespread macromolecular interaction perturbations in human genetic disorders. Cell 161, 647–660. https://doi.org/10.1016/j.cell.2015.04.013.

Sala, C., Segal, M., 2014. Dendritic spines: the locus of structural and functional plasticity. Physiol. Rev. 94, 141–188. https://doi.org/10.1152/physrev.00012.2013.

Schaefer, G.B., Bodensteiner, J.B., 1992. Evaluation of the child with idiopathic mental retardation. Pediatr. Clin. N. Am. 39, 929–943.

Schwarz, J.M., Cooper, D.N., Schuelke, M., Seelow, D., 2014. MutationTaster2: mutation prediction for the deep-sequencing age. Nat. Methods 11, 361–362. https://doi.org/10.1038/nmeth.2890.

Sells, M.A., Pfaff, A., Chernoff, J., 2000. Temporal and spatial distribution of activated Pak1 in fibroblasts. J. Cell Biol. 151, 1449–1458.

Sherry, S.T., Ward, M.H., Kholodov, M., Baker, J., Phan, L., Smigielski, E.M., Sirotkin, K., 2001. dbSNP: the NCBI database of genetic variation. Nucleic Acids Res. 29, 308–311.

Sorrell, F.J., Kilian, L.M., Elkins, J.M., 2019. Solution structures and biophysical analysis of full-length group A PAKs reveal they are monomeric and auto-inhibited in cis. Biochem. J. 476, 1037–1051. https://doi.org/10.1042/BCJ20180867.

Stockton, R., Reutershan, J., Scott, D., Sanders, J., Ley, K., Schwartz, M.A., 2007. Induction of vascular permeability: beta PIX and GIT1 scaffold the activation of extracellular signal-regulated kinase by PAK. Mol. Biol. Cell 18, 2346–2355. https://doi.org/10.1091/mbc.e06-07-0584.

Thévenot, E., Moreau, A.W., Rousseau, V., Combeau, G., Domenichini, F., Jacquet, C., Goupille, O., Amar, M., Kreis, P., Fossier, P., Barnier, J.-V., 2011. p21-Activated kinase 3 (PAK3) protein regulates synaptic transmission through its interaction with the Nck2/Grb4 protein adaptor. J. Biol. Chem. 286, 40044–40059. https://doi.org/10.1074/jbc.M111.262246.

Wang, L.W., Huang, C.C., Yeh, T.F., 2004. Major brain lesions detected on sonographic screening of apparently normal term neonates. Neuroradiology 46, 368–373. https://doi.org/10.1007/s00234-003-1160-4.

Wang, J., Wu, J.-W., Wang, Z.-X., 2011. Structural insights into the autoactivation mechanism of p21-activated protein kinase. Structure 19, 1752–1761. https://doi.org/10.1016/j.str.2011.10.013.

Wang, Y., Zeng, C., Li, J., Zhou, Z., Ju, X., Xia, S., Li, Y., Liu, A., Teng, H., Zhang, K., Shi, L., Bi, C., Xie, W., He, X., Jia, Z., Jiang, Y., Cai, T., Wu, J., Xia, K., Sun, Z.S., 2018. PAK2 Haploinsufficiency results in synaptic cytoskeleton impairment and autism-related behavior. Cell Rep. 24, 2029–2041. https://doi.org/10.1016/j.celrep.2018.07.061.

Za, L., Albertinazzi, C., Paris, S., Gagliani, M., Tacchetti, C., de Curtis, I., 2006. betaPIX controls cell motility and neurite extension by regulating the distribution of GIT1. J. Cell Sci. 119, 2654–2666. https://doi.org/10.1242/jcs.02996.

Zerbino, D.R., Achuthan, P., Akanni, W., Amode, M.R., Barrell, D., Bhai, J., Billis, K., Cummins, C., Gall, A., Girón, C.G., Gil, L., Gordon, L., Haggerty, L., Haskell, E., Hourlier, T., Izuogu, O.G., Janacek, S.H., Juettemann, T., To, J.K., Laird, M.R., Lavidas, I., Liu, Z., Loveland, J.E., Maurel, T., McLaren, W., Moore, B., Mudge, J., Murphy, D.N., Newman, V., Nuhn, M., Ogeh, D., Ong, C.K., Parker, A., Patricio, M., Riat, H.S., Schuilenburg, H., Sheppard, D., Sparrow, H., Taylor, K., Thormann, A., Vullo, A., Walts, B., Zadissa, A., Frankish, A., Hunt, S.E., Kostadima, M., Langridge, N., Martin, F.J., Muffato, M., Perry, E., Ruffier, M., Staines, D.M., Trevanion, S.J., Aken, B.L., Cunningham, F., Yates, A., Flicek, P., 2018. Ensembl 2018. Nucleic Acids Res. 46, D754–D761. https://doi.org/10.1093/nar/gkx1098.

Zhao, Z., Manser, E., Loo, T.-H., Lim, L., 2000. Coupling of PAK-interacting exchange factor PIX to GIT1 promotes focal complex disassembly. Mol. Cell. Biol. 20, 6354–6363.

Zhou, W., Li, X., Premont, R.T., 2016. Expanding functions of GIT Arf GTPase-activating proteins, PIX Rho guanine nucleotide exchange factors and GIT–PIX complexes. J. Cell Sci. 129, 1963–1974. https://doi.org/10.1242/jcs.179465.